Chapter 5

Disk-halo interaction and the plausibility of halo density laws

We investigate the effects of the disk formation on the structure of the dark matter halo. To represent the dark halos, we use N-body realizations of the $\gamma = 0$ and $\gamma = 1$ (Hernquist profile) isotropic models of Dehnen, in which the potential of a thin exponential disk is adiabatically grown. Depending on the mass and concentration of the disk, the central density gradient becomes steeper, so that the final density of the halo is well described by higher γ models. If we require the final rotation curve of the galaxy to be asymptotically flat, the range of the plausible initial halo models is narrowed considerably: only models that initially have a constant density core give flat rotation curves after the growth of the disk is complete; initial halos that follow the Hernquist profile give falling rotation curves. The $\gamma = 0$ model is shown to work equally well with the isothermal halo in this respect, without the need for an r^{-2} density profile at large radii. The initial density core of this model is converted to a cusp-like density distribution. These results deepen even further the gap between the dark halos observed in cosmological simulations and those implied by observations of the kinematics of spiral galaxies. A possible way to create a core in the final halo and have a flat or rising rotation curve is an abrupt decrease in the mass of the disk; this, however, works only for dwarf spirals that were initially very massive. For luminous spirals, the required mass loss rates are too large for this mechanism to provide a viable explanation.

1 Introduction

Dark matter halos are thought to explain the flat H I rotation curves at the outer parts of spiral galaxies, as observed for example by Bosma (1978), Begeman (1987) and Broeils (1992). They supposedly consist of collisionless, possibly non-baryonic particles that interact with the other galactic components only through gravity (see Trimble (1987) and Sanders (1990) for reviews on the subject). For lack of a better model, but also prompted by the results of early models of violent relaxation (Lynden-Bell 1967, Shu 1978) the dark halos were modeled as approximate isothermal spheres (Bahcall & Casertano 1985, van Albada et al. 1985). This kind of halo has the desired r^{-2} decrease in density at large radii

that produces asymptotically flat rotation curves, as well as a constant density core that allows the visible components of the galaxy (disk, bulge and gas) to dominate the dynamics in the inner parts. These features allowed good multi-component fits to the rotation curves of spirals (van Albada & Sancisi 1986, Kent 1987, Begeman, Broeils & Sanders 1991).

On the other hand, the most recent Cold Dark Matter (hereafter CDM) cosmological simulations (Dubinski & Carlberg 1991, Navarro, Frenk & White 1995, 1996) persistently produce halos with r^{-1} density laws at the center, and steepening to r^{-4} or r^{-3} at large radii. Such halos are referred to as "singular", since there is a central density singularity. It is still possible to obtain a good fit to the total rotation curve using these kind of singular halos (Sanders & Begeman 1994), but this applies only to large luminous spirals. The kinematics of the dark-matter dominated dwarf spirals are impossible to reconcile with singular halos (Flores & Primack 1994, Burkert 1994) and this has even prompted some authors to reject CDM halos altogether (Moore 1994).

A physical process that occurs between the proto-halo formation and the final formation of disk galaxies is the assembly of the visible stellar and gaseous disk through dissipational infall of the baryons mixed with the dark matter (Fall & Efstathiou 1980). Disk growth inside isothermal halos has been investigated analytically (Blumenthal et al. 1986, Ryden & Gunn 1987, Flores et al. 1993) as well as numerically (Barnes 1987, Blumenthal et al. 1986, van Albada & Sancisi 1986) with relatively low resolution. It was shown that baryonic infall pulls the dark matter inward destroying the constant density cores, and is quite efficient in producing final rotation curves that are flat and featureless, much like the observed ones (thus partly solving the halo-disk "conspiracy" problem—the question of how the disk and halo can be combined in such a way that there is no trace of the transition from disk-dominated region to halo dominated region in the rotation curve). The singular halos have been previously considered by Flores & Primack (1994) and Navarro, Frenk & White (1996) (hereafter NFW); they argued that baryon infall inside these halos would produce falling rotation curves, in contrast to the observations. In this paper we present high resolution numerical simulations of disk formation in these singular halos–the "Hernquist" halos, more specifically–and consider the constraints that this might put on the plausibility of certain models. The argument of Flores and Primack is confirmed, and the change in the halo density is quantified in terms of the index γ of the density models of Dehnen (1993). We also consider disk growth inside a $\gamma = 0$ halo—a model that does have an (almost) constant density core, but declines in density as r^{-4} at infinity—and show that the rotation curves resulting from this finite mass model are comparable to those of isothermal halos.

The rest of this paper is organised in the following way. In Section 2 we give a very brief description of the disk formation scenario that we adopt in this study, followed by details on the models that we use to represent the dark halos. In Section 3 we describe the effects of disk growth on the shape and the density profile of the halo, and in Section 4 the effects on the rotation curve of the galaxy. In Section 5 we consider the ability of supernova driven galactic winds to re-generate the cores that are necessary to explain the kinematics of dwarf spirals. Finally, we discuss our results and present our conclusions in Section 6.

2 Initial conditions and N-body modeling

2.1 Disk formation in CDM halos

For the formation of spiral galaxies we adopt the now classical scenario of dissipational infall as formulated by White & Rees (1978) and Fall & Efstathiou (1980). Dissipational baryonic matter is initially well mixed with the dark matter which, baryonic or not, is assumed dissipationless. The whole system has a non-zero angular momentum presumably resulting from tidal torques. The baryonic matter eventually dissipates its energy and falls toward the center of the potential well; the collapse is halted by the angular momentum, which in turn leads to the formation of a rapidly rotating thin gaseous disk.

The ratio f of visible (baryonic) to dark matter is supposed to be a universal constant and its value is constrained by primordial nucleosynthesis arguments through the relation $\Omega_b h_{50}^2 = 0.05 \pm 0.01$ (Walker et al. 1991). In this equation Ω_b is the total baryon density and $h_{50} = (H_0/50)$ km/sec/Mpc. For the standard CDM Universe with $\Omega_0 = 1$ and a Hubble constant of 75, this gives a visible to dark matter ratio $f = \Omega_b/\Omega_0 = 0.02$ as a lower limit to f. The upper limit is obtained for an open Univese with $\Omega_0 = 0.3$, for which $f = 0.10$.

The size of the final disk relative to the halo, i.e. the collapse factor, depends on the angular momentum parameter

$$\lambda = \frac{JE^{1/2}}{GM^{5/2}} \tag{1}$$

where J, E and M are the angular momentum, energy and total mass of the initial halo. The value of λ is not tightly constrained; Barnes & Efstathiou (1987) have found it to range between 0.02 and 0.1, with a mean value of $\langle\lambda\rangle = 0.05$. The ratio of the radial extent of the disk over the size of the halo (usually set by R_{max}, or truncation radius) is roughly equal to λ for f of the order of 0.05 to 0.1 (Fall & Efstathiou 1980, Flores et al. 1993).

2.2 The γ family of models

To represent the dark matter halos of spirals we would like to have models that are as close as possible to the predictions of cosmological calculations, as well as having simple analytical expressions for the density, mass, distribution function (DF) etc. Reasonable behaviour at small and large radii, i.e. finite total mass, finite rotation velocity at $r = 0$ would also be necessary. The γ-family of models proposed by Dehnen (1993) (and by Tremaine et al. (1993) as η models) fulfil most of the above requirements. The density as a function of the spherical radius is given by

$$\rho_\gamma(r) = \frac{(3-\gamma)M_h}{4\pi} \frac{a_h}{r^\gamma (r+a_h)^{4-\gamma}} \tag{2}$$

where M_h is the total mass and a_h a general scaling radius. The parameter γ takes values in the interval $0 \leq \gamma < 3$. The cumulative mass and the circular velocity as a function of

radius are given by

$$M_\gamma(r) = M_h \, (\frac{r}{r + a_h})^{3-\gamma} \tag{3}$$

and

$$v_\gamma^2(r) = \frac{G M_h \, r^{2-\gamma}}{(r + a_h)^{3-\gamma}} \tag{4}$$

respectively. As can be seen from eq. (2) the density for all the models declines as r^{-4} at large r, so that the total mass is finite, while in the center the density falls as $r^{-\gamma}$. In other words, the $\gamma \lesssim 3$ models have the steepest density gradient at the center while the $\gamma = 0$ model has an (almost) constant density core. The models of Jaffe (1983) and Hernquist (1990) correspond to $\gamma = 2$ and $\gamma = 1$ respectively. In Fig. 1a-1c we give the density, mass and circular velocity profiles for $\gamma = 0$, 1 and 2. The total mass in all the cases is set equal to 1, as well as the radial scale a_h, and this means that the models shown in Fig. 1 are *not* normalized in radius; i.e., the half mass radius of the $\gamma = 0$ halo is $3.84 a_h$, while for the Hernquist halo $r_{1/2} = 2.41 a_h$.

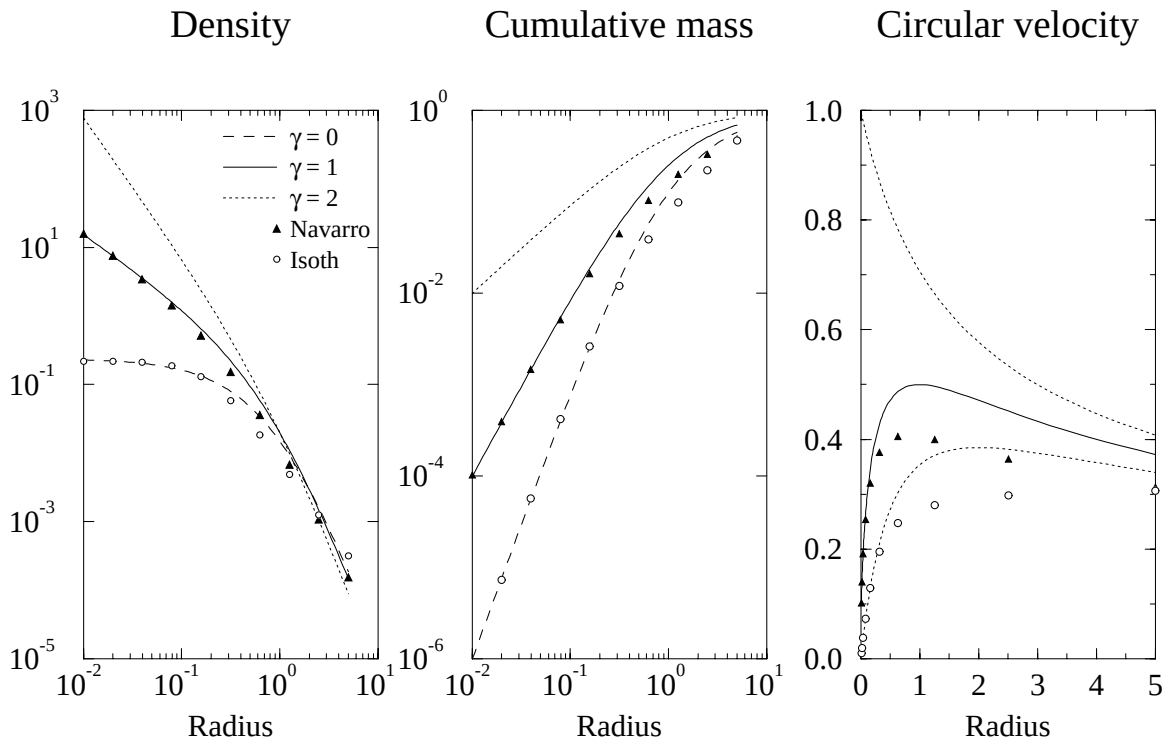

Figure 1: Density, cumulative mass and circular velocity profile of the γ-models of Dehnen, and of the non-singular isothermal sphere and the NFW halo model (see text). The isothermal profile is normalized to the same central density as the γ_0 model, and the NFW profile is normalized to a total mass of 1 at $r = 100$. For all γ-models, $a_h = M_h = 1$.

As mentioned earlier, the gravitational collapse of density peaks as simulated by Dubinski & Carlberg (1991) produced dark halos that are very well described by the Hernquist model, from the softening radius outward. The CDM halos emerging from the most recent

simulations have profiles that are identical to the Hernquist profile in the central regions (NFW) but with a total mass that diverges logarithmically, i.e.

$$\rho(r) = \frac{M_c}{4\pi a} \frac{a}{r\,(r+a)^2} \tag{5}$$

where M_c is the mass inside an arbitrarily chosen cutoff in r. In Fig. 1 we plot the density etc. of the NFW model normalized to the density of the Hernquist ($\gamma = 1$) model in the inner regions, and to a total mass of unity at $r = 100$. The main difference between the two is the behaviour at large radii; the Hernquist models falls off as r^{-4} while the NFW model as r^{-3}. At small radii the two distributions are almost indistinguishable. In the same figure we also plot the density of the non-singular isothermal sphere with a core radius r_c of unity and scaled to the central density of the γ_0 model. For this plot we use the approximate empirical profile $\rho(r) = \rho_0/(1+(r/r_c)^2)$ that has become the standard representation of an isothermal halo. As can be seen in Fig. 1 the $\gamma = 0$ model (from this point on referred to simply as γ_0) is a relatively good approximation to the isothermal sphere in the sense that it also has a core, while its mass is finite. The "core radius" of the Dehnen model, i.e. the radius where the density has fallen to half its central value would be $r_c^\gamma \approx 0.20$, for $a_h = 1$. In this paper we will not discuss isothermal models, since they have been considered previously (van Albada & Sancisi 1986, Barnes 1987).

2.3 N-body setup

In the present paper we consider primarily isotropic spherical halos. Anisotropic halos of Ossipkov-Merritt type, where the distribution function depends in a certain way on the energy and the angular momentum, will be considered separately. The inherent stability of these models depends very sensitively on the degree of anisotropy, and the parameter space that needs to be explored is too large for the purpose of this study. Therefore, only a few cases are described, in Appendix A. The assumption of spherical symmetry of the initial halos, on the other hand, is really an oversimplification, dictated mainly by computational limitations. The halos in the simulations of Dubinski & Carlberg, for example, are significantly flattened, and often triaxial. The general nature of the response of the density distribution, however, is not expected to be very different than that of the simple spherical models (Flores et al. 1993).

The construction of the N-body halos is straightforward, owing to the availability of analytical expressions for the density and the distribution function. First, a spherical radius is assigned to each particle by modulating an ensemble of random numbers according to the inverse expression for the cumulative mass. Then, using the acceptance-rejection method, a velocity is assigned to each particle according to the value of the DF at that particular radius. The models that we use in this study consist normally of 66,000 particles. A few runs are made using 120,000 particles; an N of this order is necessary for reliable axis ratio determination at small radii. As before, the total mass of the halo and the radial scale a_h are both set to 1.

The baryonic infall is simulated by slowly turning on the potential of a thin exponential disk whose surface density increases with time. It is assumed that the initial total mass

of the system includes both dark and baryonic matter in uniform mix and therefore, as the mass of the disk increases, an equal amount of mass is *subtracted* from the dark halo at each time step. In practice this is done by simply setting the mass of a random halo particle to zero. The masses used for the disk span a range of plausible visible-to-dark matter ratios, from $f = 0.03$ to $f = 0.1$. For each value of the disk mass, 3 values of the disk scalelength are applied, ranging from 0.05 to 0.15 in units of a_h. These values are suggested by angular momentum constraints; as mentioned in §2.1, the ratio of disk to halo scale according to the tidal torque theory is of the order of 0.05, with an uncertainty of roughly a factor of 2. The halos in this study do not really have a cutoff radius, but if we approximate it by the radius enclosing 90% of the mass, then for a Hernquist halo $\mathrm{R}_{max} \approx 20a_h$. Taking the radius of the disk to be 5 exponential scalelengths, the ratio h_d/a_h should have a mean value of 0.10. In addition to this rough *ab initio* calculation, these values for the disk scalelength are also suggested by the ratio h_d/a_h resulting from non-linear fits of Hernquist halos plus disks to the H I rotation curves of spirals (Sanders & Begeman 1994). These ratios lie in the range 0.04 to 0.1, which, assuming that the a_h of the initial halo has not changed more than $30-40\%$ implies initial scalelength ratios of the order of 0.03 to 0.08. (This assumed change, of course, remains to be justified by the results of the simulations!). Finally, an upper limit to the disk parameters is provided by the requirement that the combination of mass and scale of the disk should not give a central surface brightness higher than the upper cutoff of $20.5\,B\mathrm{mag/arcsec}^2$ observed in spirals (de Jong 1995). Assuming a disk mass to light ratio of 1 $M_\odot/L_\odot$ in the B band, this cutoff corresponds to a maximum central surface density of $\Sigma_0 \approx 4 \times 10^8 M_\odot/\mathrm{kpc}^2$. We have that

$$\Sigma_0 = \frac{M_d}{2\pi h_d^2} = \frac{f M_h}{2\pi(\xi a_h)^2} \tag{6}$$

where f is, as before, the visible to dark mass ratio and ξ is the desired scalelength ratio. Assuming a typical halo mass $M_h \approx 10^{12}$ $M_\odot$, and an average value for a_h of 50 kpc, (Sanders & Begeman 1994), equation (6) gives a minimum value of $\xi_{\min} = 0.12$ for $f = 0.10$ or $\xi_{\min} = 0.06$ for $f = 0.03$. These values are, admittedly, subject to many assumptions and do not give really tight constraints, but they allow us for example to reject a disk with a mass of $0.1M_h$ and an h_d of $0.05a_h$ as too dense in the center.

It is also important that the disk growth takes place adiabatically. In this way, the final state of the system depends only on the final values of the mass and extent of the disk and not on the specific way that it was assembled. The total mass of the disk is grown exponentially to its final value as $M_{disk}(t) = M_d(1-\exp(t/\tau))$, while the scalelength h_d is kept fixed. The exponential growth is clearly a matter of preference; adiabaticity guarantees that the results will remain the same if the increase is, for example, linear. In the simulation system of units $G = M_h = a_h = 1$ the disk growth timescale τ is taken to be 10 units. The dynamical time scale of a Hernquist halo, for instance, at radius r, is given by

$$t_{dyn} = \sqrt{\frac{3\pi}{16G\rho}} = \frac{\pi}{2}\sqrt{r}(r+1) \tag{7}$$

At $r = 0.5a$, roughly the limit of the disk, the above formula gives a dynamical time of

1.6 units. This is about six times smaller than the disk growth time, in accordance with adiabaticity.

2.4 The self-consistent field code

For the evolution of the halos we use a Self-Consistent Field (SCF) N-body code (Hernquist & Ostriker 1992), kindly provided by Lars Hernquist. It is an "expansion" code, as opposed to direct N-body schemes such as treecodes and direct summation. The Poisson equation is solved by expanding the density and the potential in a set of basis functions, both radially and azimuthally. In this respect, it is analogous to the spherical harmonics expansion scheme developed by van Albada & van Gorkom (1977). Using the SCF code the CPU cost scales as $O(N)$ instead of $N \log N$ of the treecode, but at the price of a restricted range of models that this scheme can handle: The generic expression for the expansion of the density is

$$\rho_{nlm}(r) = \frac{K_{nl}}{2\pi} \frac{r^l}{r(1+r)^{2l+3}} W_{nl}(\xi) \sqrt{4\pi} Y_{lm}(\theta, \phi) \tag{8}$$

where K_{nl} are normalization constants, $W_{nl}(\xi)$ is a set of orthogonal polynomials and Y_{lm} are the spherical harmonics. As can be seen, the zero-th order radial basis function used for the expansion is the Hernquist (1990) profile. Therefore, for the expansion to converge using a reasonable number of terms, the system must not be too far away from this kind of density distribution. The same applies to the azimuthal terms; the system under consideration should not be too far from spherical symmetry. Ideally, it should be a perturbation about the spherical Hernquist model. Hernquist & Ostriker (1992) have shown that by including a sufficient number of expansion terms, this scheme can also very well describe models with constant density cores. Since in this study we are concerned with exactly these two kinds of systems, the SCF scheme is very well suited for our purpose. In most of the runs we use 6 radial and 4 azimuthal expansion terms. The convergence of the expansion is monitored continuously, however, and for the most extreme perturbations–massive extended disks–we use radial terms of up to $n = 10$. A typical run of 3000 time steps employing 66,000 particles and using $n_{max} = 6$ and $l_{max} = 4$ takes 4 hours on an Ultra Sparc workstation. Self-evolution runs are made for both halo models used in this study; in these runs the energy is conserved to better than 0.1%, and the systems are stable. The only perceptible change is a correctable displacement of the center of mass, as noted also by Hernquist & Ostriker (1992).

3 Effects of the disk field on the halo density

3.1 The shape of the halo

We first address the issue of whether the three dimensional shape of the halo changes significantly as a result of the disk force field. It has been claimed by van Albada & Sancisi (1986) and Barnes (1987) that the halo does not become perceptibly flatter; however, their simulations, using 5000 and 4000 particles respectively, did not have sufficient resolution

to detect changes in ellipticity at small radii, where they would supposedly be largest. We utilize a Hernquist halo of 120,000 particles for two runs, with an h_d of $0.1a_h$ and $0.05a_h$. The ratio of visible to dark mass is fixed to $f = 0.05$. In these runs and in the ones that follow, the halo particles are first allowed to relax, and then the disk field is turned on using a standard timescale of 10 units. The simulation is run until $t = 40$, when the disk has reached about 98% of its asymptotic mass. In practice, the halo has already reached equilibrium at around $t = 25$. The same runs are repeated for a γ_0 halo and the axis ratio (c/a) is then measured as a function of radius. The axis ratio is calculated using the method proposed by Dubinski & Carlberg (1991) and Katz (1991) by diagonalizing the inertia tensor of the system; the reader is referred to these papers or to Chapter 4 of this thesis for more details. Using an N of this order, the ellipticity can be measured to an acceptable accuracy (5−10%) already at $r \approx h_d$ where approximately 1000 particles are included. As the number of enclosed particles grows the accuracy increases rapidly, and becomes better than 0.5% for N of the order of 10^4 (for some tests regarding the accuracy of this method, see Appendix B). The resulting axis ratio as a function of radius is shown in Fig. 2a and 2b, for $\gamma = 1$ and $\gamma = 0$. The high level of noise in the γ_0 model is due to the constant density core at the center, which implies a very small number of particles there. The flattening of the halo is not large but definitely not negligible, reaching a value of $c/a = 0.70$ for both kinds of halos, at about 3 disk scalelengths from the center. According to the results given in Appendix B, however, the true flattening might well be even greater to the center, since the algorithm always underestimates the ellipticity in regions with a small number of particles.

As one would expect, the effects of more extended disks are smaller and appear at larger radii. In general, the halo does not regain its spherical shape until about $8h_d$ from the center; within the Holmberg radius the axis ratio is still around 0.85. It should be stressed here that these axis ratios refer to *all* the particles inside the particular radius, and not to a thin shell. This means that the flattening of a certain equidensity shell at, say, $3h_d$ can be higher than the value in Fig. 2. These values, of course, are not comparable to the very high ellipticities found for example by Sackett & Sparke (1990) in polar ring galaxies. They do show, however, that the mere existence of a stellar disk means that the surrounding halo is not spherical, at least in the inner parts.

3.2 The density distribution

Now we consider the changes in the density distribution of the halo. The main diagnostic used is the cumulative mass profile, rather than the density itself. This integration over density increases the signal-to-noise considerably, smoothing out the discreteness noise and allowing much more reliable fits. According to the order-of-magnitude calculations in §2.3, we use a 3×3 grid in disk parameters: the disk-to-total mass ratio takes the values 0.03, 0.05 and 0.1, while the exponential scalelength is taken to be 0.05, 0.08 and 0.15 in units of a_h. These 9 combinations are run for both halo models ($\gamma = (0, 1)$), and some additional runs are made using more extreme parameter values: A very diffuse disk with a mass of $0.03M_h$ and a scalelength h_d of $0.25a_h$ in a γ_0 halo, and an equally large disk but with a mass of $0.10M_h$ in a Hernquist halo. The density and mass profile of the final state of the

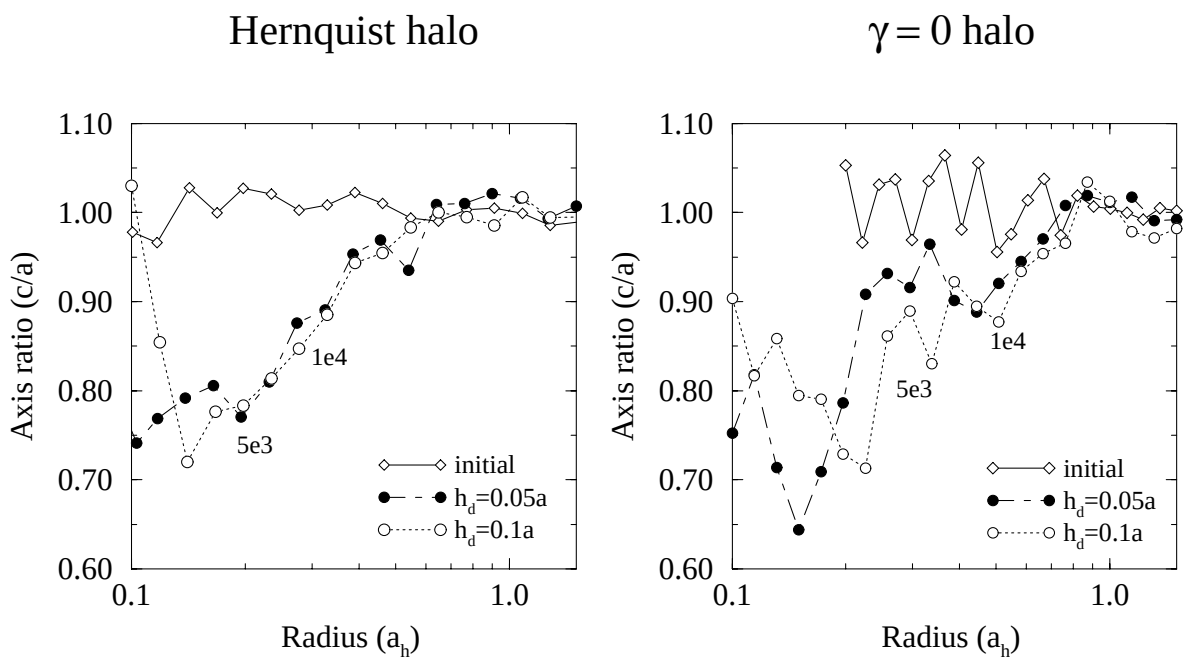

Figure 2: Axis ratio as a function of radius before and after the growth of the disk for the two types of halos, and for two different disk scalelengths. The mass of the disk is $0.05 M_h$ in all these runs. The approximate radii that include 5000 and 10000 particles are indicated.

halo are measured by counting the number of particles inside ellipsoidal volumes, based on the run of ellipticity as a function of radius. The correction with respect to spherical shape is small, but essential for a consistent description. For simplicity, and also because of the rather noisy actual ellipticity profile, the axis ratio is taken to increase linearly from a value of ≈ 0.7 at the center to 1 at $5h_d$ and remain constant from there on. In Fig. 3a and 3b we give the final density and mass distributions for a disk mass of $0.05\ M_H$ and for the largest and smallest scalelengths, 0.05 and $0.15a$ for a Hernquist and a γ_0 halo.

The change in the density and mass profiles is obvious, and especially the replacement of the central core by a steeply rising density distribution in the γ_0 model. It is also relatively easy to see that a profile of the original form, Hernquist or γ_0 , cannot give a satisfactory description any more, since the density at large radii still falls as r^{-4}, but in the center it is steeper than the respective r^{-1} and r^0 density laws of these two models. Something more versatile is needed for a good description, and the γ models provide this, through their functional form. We fit the mass profiles using eq. (2), but treating γ as a free parameter. As can be seen in the lower panels of Fig. 3, this is an effective way of representing the mass distribution. There are some discrepancies at radii smaller than $0.07a_h$ but these are mainly due to the small number of particles (a few hundred) in these regions. For the compact disk the best-fit γ is 1.47, meaning that the initial Hernquist profile lies now between a Hernuist and a Jaffe model in terms of central density gradient. The more diffuse disk gives, as expected, a γ of 1.04, much closer to the initial value of 1.0. The profiles shown in Fig. 3 extend out to $1a_h$, as well as the fits. The best-fit γ is not sensitive to the radial range used; the difference is not more than $\Delta\gamma = 0.1$ if we take,

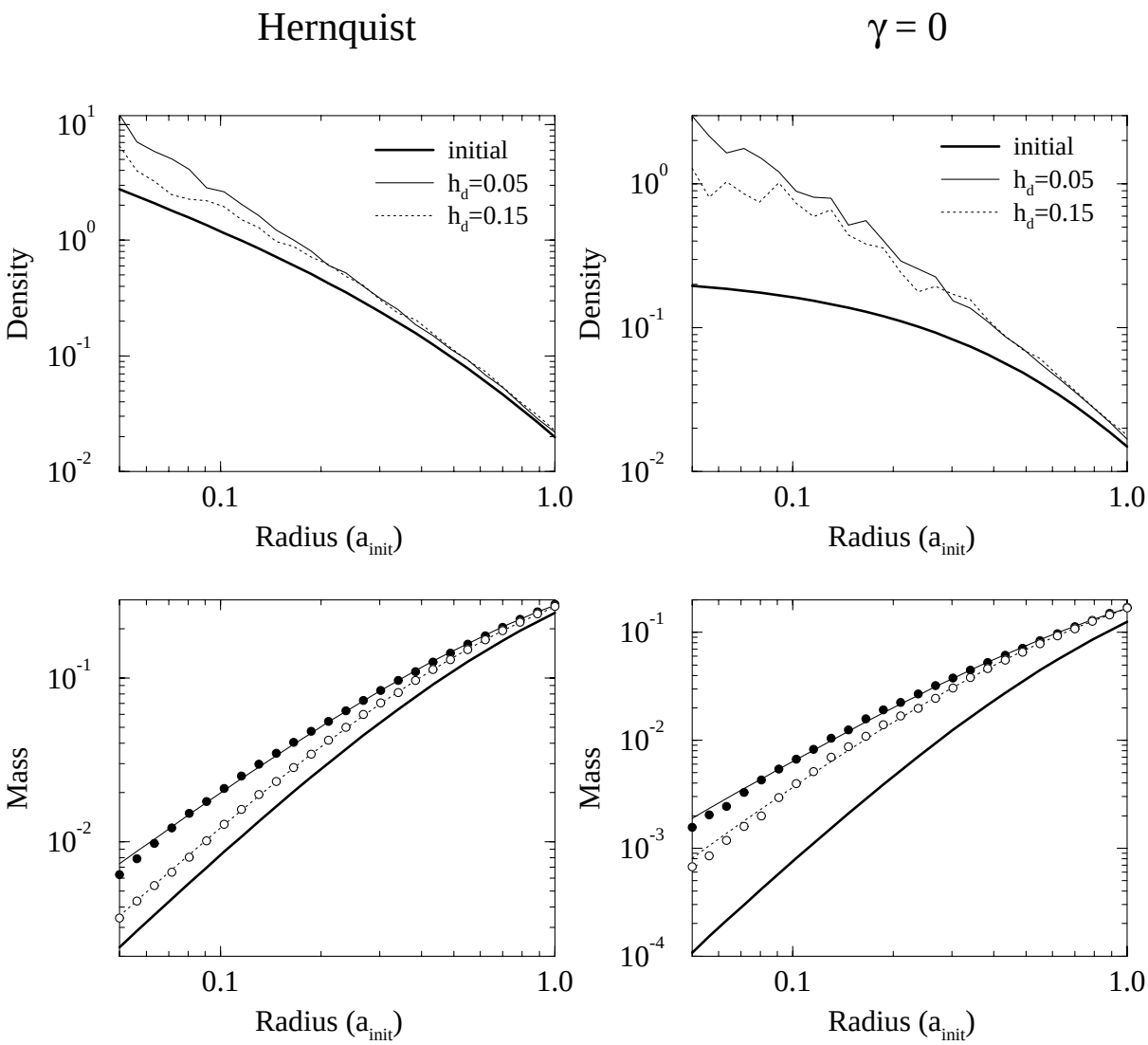

Figure 3: *Upper panels:* Effects of disk growth on the density profile for the two types of halos discussed in the text. The mass of the disk is $0.05M_h$. *Lower panels:* Mass profile of the same models as above. Filled circles correspond to h_d=0.05, open circles to h_d=0.15 in units of initial a_h. The thin solid and dotted lines show the best-fit γ-profile.

for instance, a "disk-dependent" limit of 10 or 20 disk scalelengths. The typical error in γ given by the fitting routine is of the same order or less, and so the total error is of the order of 5–10%.

The results for all 9 models of the simulation are given in columns (4) and (3) of Tables 1 and 2 respectively. In general, for a given disk mass, smaller scalelengths give force more halo material to accumulate in the center, thus giving higher final γ values. As an indication of the degree of shrinking of the halo we give the halo mass inside the Holmberg radius of the galaxy (taken to be $R_{Hol}=4.5h_d$) before and after infall, in columns (5-6) and (4-5) of Tables 1 and 2. The increase is a factor of 1.5−2 for the Hernquist halos and 2−4 for the γ_0 halos. In column (3) of Table 1 we also give the best-fit a_h of the final halo, by fitting a Hernquist profile to it. This value is only indicative of the amount of shrinking

of the halo; it is *not* the real scale radius of the halo, since, as we mentioned already, the Hernquist profile is no longer a good description of the density of the halo. Depending again on the disk concentration, a_h is reduced by 10-30%. In column (7) (Table 1) and (6) (Table 2) we give the ratio of visible to dark matter inside the Holmberg radius ($f_{\rm Hol}$) of the galaxy. This quantity is of some importance, since it has been used extensively as a measure of the relative contribution of dark matter to the dynamics of individual galaxies. For the Hernquist halos, $f_{\rm Hol}$ lies between 0.15 and 0.75, for γ_0 between 0.4 and 2.7. The implications of these values will be considered in the Conclusions Section. Finally, in column (8) (Table 1) and (7) (Table 2) we give the final form of the rotation curve and the dominant component at small and large radii.

Table 1: Results of the Hernquist model.

M_d (1)	h_d (2)	a_h (3)	γ (4)	M_{init} (5)	M_{fin} (6)	$f_{\rm Hol}$ (7)	Rot. curve (8)
0.03	0.05	0.80	1.44	0.03	0.05	0.50	$\searrow$ (DH)
	0.08	0.82	1.32	0.07	0.09	0.28	$\searrow$ (HH)
	0.15	0.84	1.01	0.16	0.18	0.14	$\searrow$ (HH)
0.05	0.05	0.74	1.47	0.03	0.06	0.75	$\searrow$ (DH)
	0.08	0.78	1.24	0.07	0.10	0.45	$\searrow$ (DH)
	0.15	0.82	1.04	0.16	0.25	0.18	$\searrow$ (HH)
0.1	0.05	model too dense					
	0.08	0.67	1.31	0.07	0.12	0.75	$\searrow$ (DH)
	0.15	0.73	1.12	0.16	0.29	0.25	$\searrow$ (HH)
	0.25	0.79	0.98	0.28	0.30	0.29	$\searrow$ (HH)

Columns in Table: (1) Mass of the disk (baryons) **(2)** Disk scalelength **(3)** Best-fit *Hernquist* scale radius (a_h) of the final halo (indicative; see text) **(4)** Best-fit γ of the *final* halo **(5)** Fraction of the total dark matter inside the Holmberg radius *before* baryonic infall **(6)** Same as (5), after infall **(7)** Final ratio of visible to dark matter inside the Holmberg radius **(8)** Shape of the rot. curve in the region 7−10 disk scalelengths: $\longrightarrow$ flat; $\searrow$ falling. In parentheses, the dominant component at small and large radii. D for Disk, H for Halo

4 Effects of the disk field on the rotation curve

The most crucial test of a halo model is the predicted rotation curve, since this is currently the only tracer of the force law in the outer regions that can be measured accurately. HI rotation curves have been traced out to 10 disk scalelengths or more (Begeman 1987), providing a firm basis for tests of halo models. The performance of Hernquist halos in the context of the form of the rotation curve after baryonic infall has been considered by Flores & Primack (1994), Burkert (1994) and Moore (1994). Using simple theoretical arguments

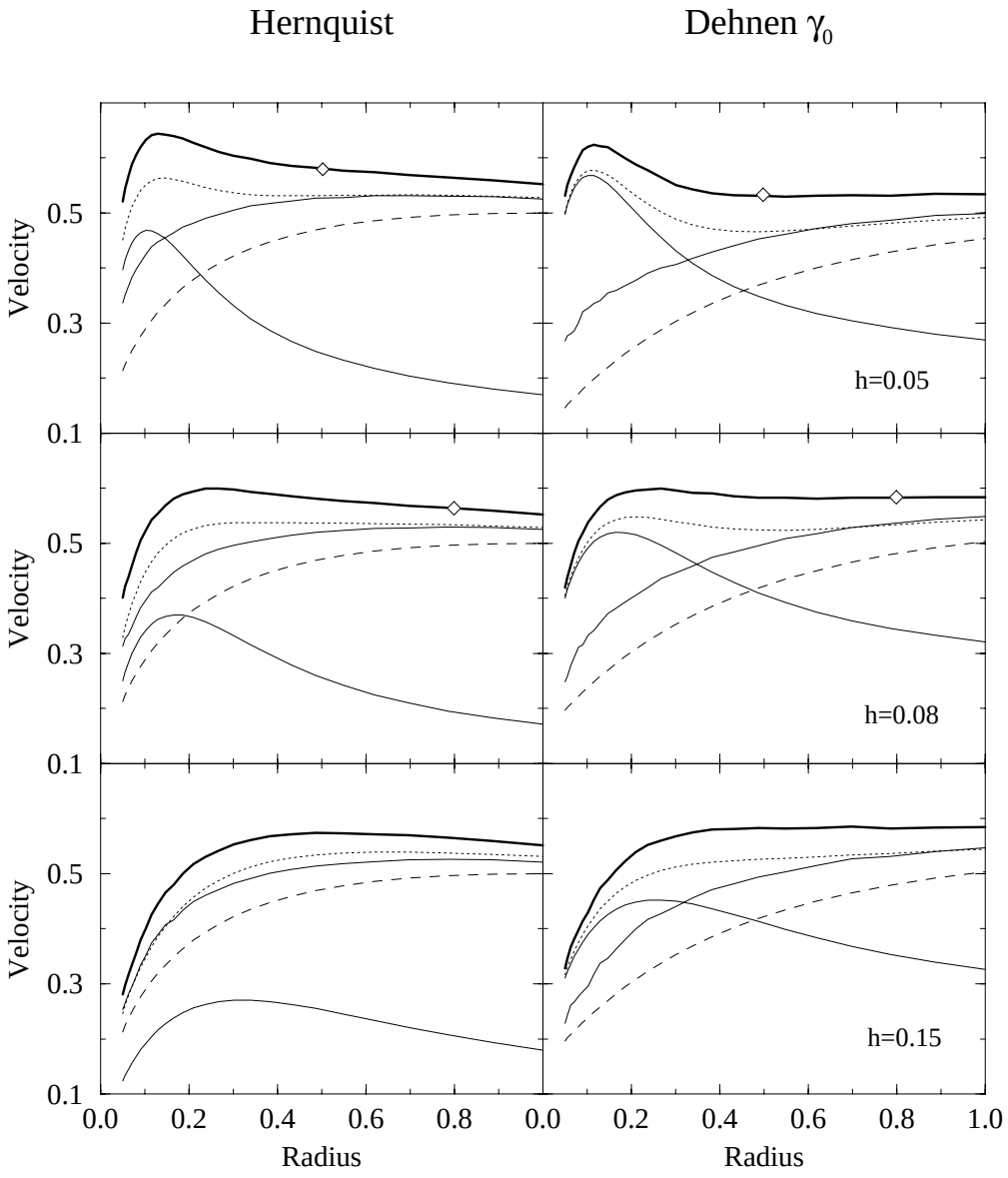

Figure 4: *Left panels:* Rotation curves for the Hernquist halos. The mass of the disk in these plots is $0.03M_h$, and the scalelength is, from top to bottom, 0.05, 0.08 and 0.15 in units of initial a_h. Thick solid line: Total rotation curve (halo + disk) after the disk growth is complete. Thin solid lines: Individual disk and halo rotation curves. Dashed line: Halo rotation curve before disk growth. Dotted line: Total "no-interaction" rotation curve, obtained by quadratically adding the halo r.c. before disk growth, to that of the disk (lower solid line + dashed line). The diamonds mark the $10h_d$ point, usual outer limit of the observed H I rotation curves. In the bottom graph, it lies beyond the boundary. The velocity units are conventional. *Right panels:* Same as before, for the γ_0 halo.

Table 2: Results of the γ_0 model.

M_d (1)	h_d (2)	γ (3)	M_{init} (4)	M_{fin} (5)	$f_{\rm Hol}$ (6)	Rot. curve (7)
0.03	0.05	1.24	0.006	0.018	1.45	$\longrightarrow$ (DD)
	0.08	0.70	0.018	0.036	0.73	$\longrightarrow$ (DH)
	0.15	0.27	0.043	0.067	0.40	$\longrightarrow$ (DH)
	0.25	0.25	0.140	0.170	0.15	$\longrightarrow$ (HH)
0.05	0.05	1.13	0.006	0.024	1.78	$\searrow$ (DH)
	0.08	0.89	0.018	0.045	0.97	$\searrow$ (DH)
	0.15	0.64	0.043	0.076	0.57	$\searrow$ (DH)
0.1	0.05	0.92	0.006	0.032	2.73	$\searrow$ (DH)
	0.08	0.94	0.018	0.059	1.48	$\searrow$ (DH)
	0.15	0.48	0.043	0.093	0.95	$\searrow$ (DH)

Columns in Table: **(1)** Mass of the disk (baryons) **(2)** Disk scalelength **(3)** Best-fit γ of the *final* halo **(4)** Fraction of the total dark matter inside the Holmberg radius *before* baryonic infall **(5)** Same as (4), after infall **(6)** Final ratio of visible to dark matter inside the Holmberg radius **(7)** Shape of the rot. curve in the region 7–10 disk scalelengths: $\longrightarrow$ flat; $\searrow$ falling. In parentheses, the dominant component at small and large radii. D for Disk, H for Halo

as well as secondary indirect evidence, these authors argued that a halo with a Hernquist profile would give a falling rotation curve after the growth of the disk. These halos work quite well in the decomposition of H I rotation curves (Sanders & Begeman 1994), but this includes the explicit assumption that the halo has a Hernquist form after the disk has been formed. As we showed in the previous section, a halo that had this form initially will have a steeper density distribution after baryonic infall, and hence can no longer be described by the same law. The halo rotation curves are determined by calculating the mass inside *spherical* shells, and then using the Keplerian expression $v_c^2 = GM(r)/r$. Ellipticity corrections have been omitted, since the ellipticities of these systems have a maximum value of around 0.25; the corresponding difference from a spherical rotation curve is very small (Binney & Tremaine 1987, p.59) and the calculation involves time-consuming integrations of the density to infinity. Taking the ellipticity into account, the rotation curves would be slightly more peaked at the center. In the left panels of Fig. 4 we give all the components as well as the final rotation curve of a Hernquist halo. The disk has the same mass in all three cases, M_d= 0.03, and the scalelength is 0.05, 0.08 and $0.15a_h$. We also show the rotation curves of the disk, the halo before infall, the final halo and an "no-interaction" rotation curve, that results by adding the contribution of the disk and the initial halo, as if no interaction has taken place. We also mark the radii at $10h_d$, to give an idea of the observable range of the particular rotation curve. The basic feature in these plots is obvious: The final rotation curves after they peak at around 2–$3h_d$, are declining continuously; they do not have a flat part at all. It is interesting to notice that the first two "no-interaction"

curves do have a significant flat part, which is destroyed by the disk-halo interaction. The mass distribution of the halo is such that as the disk pulls material inward, the total mass will always give a declining rotation curve. It is also important to stress that this is not a problem of fine-tuning; if it were, we should observe rising rotation curves also, and flat ones would be possible by adjusting the parameters properly. The problem lies within the Hernquist profile itself. In the left panel of Fig. 5 we give all 9 rotation curves of this model, grouped by disk mass. It is again obvious that, covering all possible values of mass and scalelengths ratios, it is not possible to obtain a flat rotation curve, such as the ones observed in most of the intermediate- and a number of the high-luminosity spirals.

The situation is different when we consider the γ_0 halo. In the right panels of Fig. 4 we show the same configurations as before. This time, however, all three rotation curves have a significant flat part. Only in the first rotation curve, with an h_d of 0.05, is the flat part mostly outside the observable radius of $10h_d$. The other two are flat from $4h_d$ outward. It is also interesting that the "no-interaction" rotation curves are nowhere flat. The first two are declining at radii where the disk dominates and then rising when the halo takes over, thus also displaying a disk-halo transition region. The third one (h_d=0.15) is rising at all radii. This suggests that if the visible to dark mass ratio is 0.03, and if the primordial halos have a form similar to that of the γ_0 model—i.e. with a large core—the "conspiracy problem" is solved to a certain degree: The disk halo interaction during the collapse of the former erases any obvious transition region, and also creates a flat rotation curve over a large range of radii, where before there was none. This is in agreement with the results of Blumenthal et al. (1986) and Barnes (1987) for the rotation curves of isothermal halos. In the right panel of Fig. 5 we give the rotation curves of all 9 runs. For f of 0.05 and 0.1, the rotation curves are declining throughout. We should also notice that rising rotation curves such as those observed in dwarf and Low Surface Brightness galaxies (de Blok et al. 1996) cannot be produced by either of the two models used in this study. Even a very diffuse disk in a γ_0 halo gives a total rotation curve that is flat beyond $3h_d$, and even begins to decline slightly at around $8h_d$.

It should be mentioned that declining rotation curves are not unusual in bright, rapidly rotating spirals (Casertano & van Gorkom 1991) Therefore, this should not constitute grounds to dismiss a certain model. We do demand, however, that the model of choice should also be able to produce flat and featureless rotation curves, such as the ones observed. Finally, it might be worthwhile to highlight a coincidence. The (initial) γ_0 model that gives the flat rotation curve for h_d=0.08 in Fig. 4 is, at the end of the simulation, almost a Hernquist model (from Table 2, $\gamma = 0.7$). However, this Hernquist halo does not arise from the CDM initial conditions, but from an "infall-modified" non-singular halo. This would be able to explain the successful fits of Hernquist models to rotation curves of luminous spirals by Sanders & Begeman (1994), and also the failure of these models in the dwarf galaxies. Again, if the initial halos are non-singular, and have a large core, the assembly of large luminous disks inside them would convert them into approximate Hernquist models.

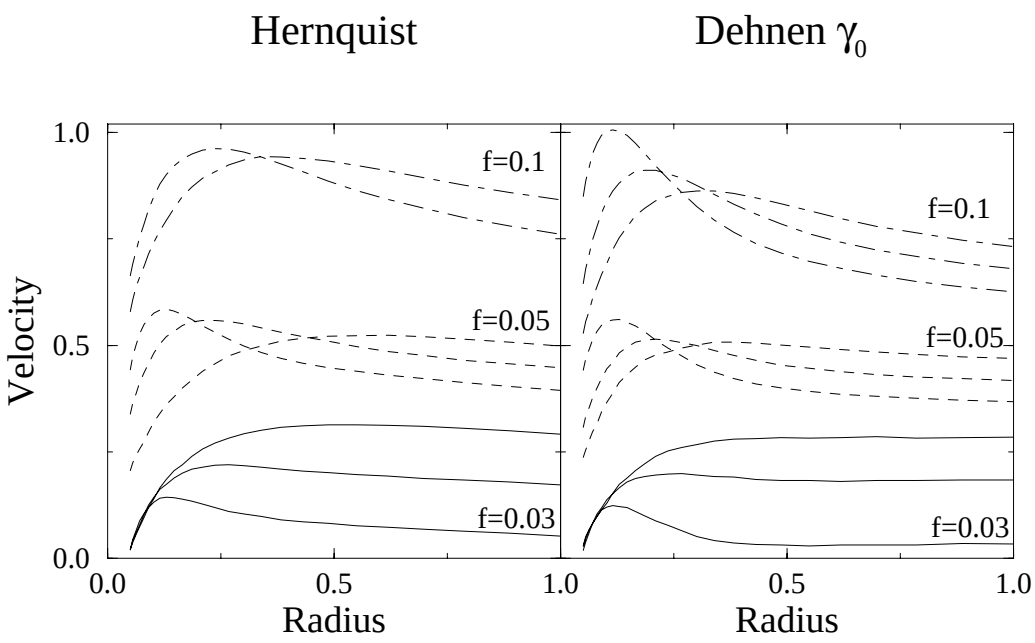

Figure 5: All the rotation curves for each halo model, shown together. The curves are grouped together by visible to dark matter ratio (f), and each one is arbitrarily shifted vertically for clarity.

5 Baryonic blow-out as a means to create a core

In Sections 3 and 4 we conclude that the steep density gradient of the CDM halos makes it impossible to create a rotation curve that is flat, after the baryonic infall. A very crucial test for any halo model is the comparison with the rotation curves of dwarf galaxies. These galaxies have a very small baryonic content; the classical dwarf spiral DDO 154 according to a "maximum disk" fit has a stellar mass of $M_\star = 0.01 \times 10^{10} M_\odot$ (Broeils 1992). This quantity of visible mass is unable to account for the rotational velocity at any radius, and therefore these galaxies are thought to be dark-matter dominated at all radii. The typical rotation curve of a dwarf spiral rises linearly from the center, implying the existence of a core in the halo density, and again being in sharp contrast with the singular structure of the CDM halos (Burkert 1994, Moore 1994). A possible way to reconcile these two effects is found in the very process that is supposed to create a dwarf spiral. These galaxies are thought to have low visible mass at the present time not because of being initially poor in baryons, but because most of the baryons were expelled from the galaxy at an early stage, through supernova-driven mass outflows (Dekel & Silk 1986). This process is likely to affect the structure of the inner halo, and might be able to produce the desired core in the density. Navarro, Eke & Frenk (1996) (NEF) made some simulations similar to the ones in this paper to investigate this. Using Hernquist initial halos, they found that it is indeed possible to create a core in the center: if the disk field is removed abruptly from a halo-disk equilibrium configuration, the halo tends to acquire its initial profile before the disk growth, i.e. the Hernquist form. Because the process is non-adiabatic, however, the halo "overshoots" the Hernquist profile and the final density distribution is less steep than

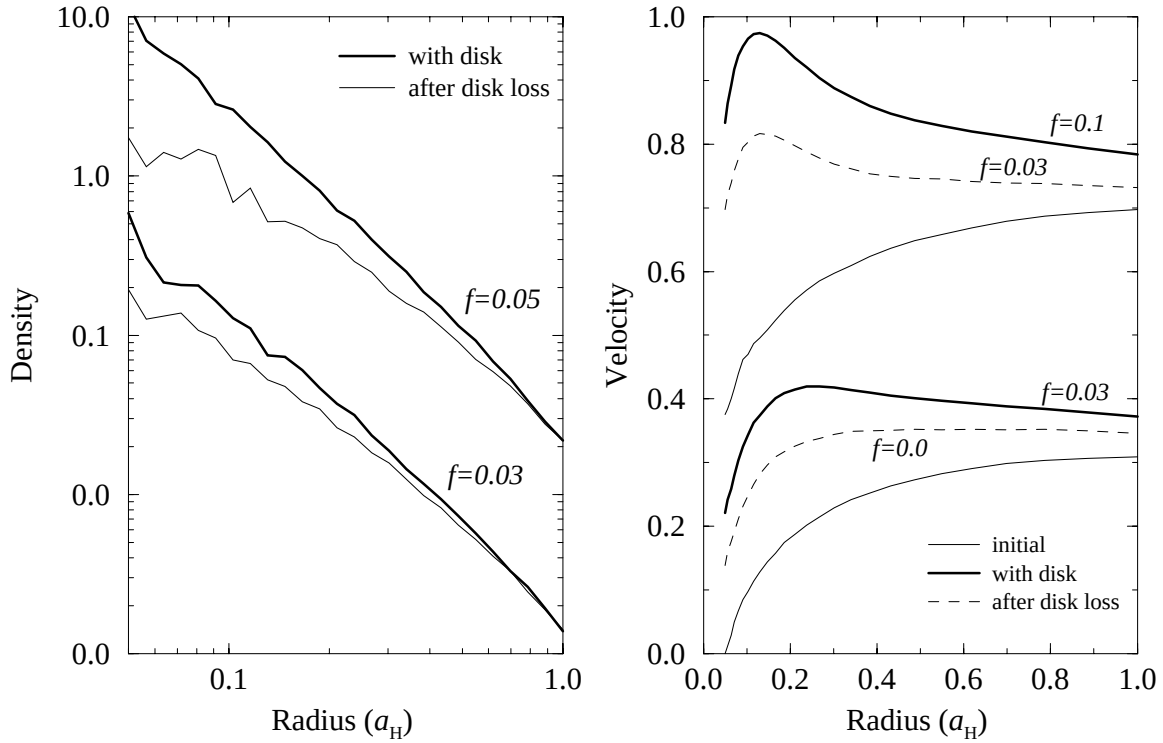

Figure 6: *Left panel:* The effects on the halo density of blowing away all the mass of the disk. Thick solid lines: Halo density after the growth of the disk is complete. Thin solid lines: Halo density after the disk has been abruptly blown away. *Right panel:* The total rotation curve of the galaxy, after blowing away a part or all of the disk. Thin solid lines: Initial rotation curves of halo only. Thick solid lines: Total rotation curve (halo + disk) after the disk growth is complete and the system is in equilibrium. Dashed curves: Total rotation curve after all (lower plot) or only a part (upper plot) of the disk has been blown away. The vertical separation of the results for the two models, with initial M_d=0.03 and M_d=0.1 is arbitrary.

r^{-1}. The values of the disk parameters used by NEF are only marginally compatible with angular momentum and baryon mass fraction constraints. They used disk scalelengths of 0.01, 0.02 and $0.04a_h$and masses of $0.05{-}0.2M_h$– i.e., the initial disks that were blown away are both too compact and too massive, especially in view of the fact that, in their calculations, density cores are created only for M_d>0.1 and h_d= 0.01.

Here we extend the parameter space covered by NEF to the parameter space described in previous sections of this paper. We follow the same procedure as NEF for a light diffuse disk and a massive compact one, using the combinations (M_d, h_d) = (0.03, 0.08) and (0.05, 0.05). These simulations begin at the point in time where those of Section 3 stopped; at that certain moment the disk field is turned off completely and the halo is left to seek a new equilibrium. In addition to this, we repeat the procedure allowing the disk to keep a fraction of its original mass; one would expect that, very roughly, this could have happened to a number of luminous spirals, that did not lose enough mass through outflows to be called dwarfs. For this experiment we use two sets of disk parameters, (M_d, h_d) = (0.03,

0.08) and (0.1, 0.05). In the first case the disk loses half its mass and in the second two thirds of its mass.

Table 3: Parameters of the mass-loss runs

# (1)	M_d^i (2)	h_d (3)	M_d^f (4)	γ (5)	Rot. curve (6)
1	0.03	0.08	0.00	0.81	Rising
2	0.05	0.05	0.00	0.75	Rising
3	0.03	0.08	0.015	0.87	Flat
4	0.1	0.05	0.03	0.92	Flat

Columns in Table: (1) Reference number for the run **(2)** Initial disk mass **(3)** Disk scalelength **(4)** Final mass of the disk **(5)** Best-fit γ of the final halo **(6)** Shape of the rotation curve in the region 7−10 disk scalelengths

The results are shown in Fig. 6. It is obvious that also with these values of disk mass and scalelength the halo rebounds in the same manner observed by NEF in their simulations. The density of the final halo—after the disk is lost—is shallower in the center than the initial halo (before disk formation). The new density profile does not acquire a constant density core. Quantified in terms of γ, the smallest value attained by the shape of the profile is $\gamma = 0.75$, i.e. the profile is still rather steep in the center. However, the remaining—pure halo—rotation curve is not very much different than those of dwarf spirals. It would be of interest to see whether these rotation curves can be fit with, say, models having a γ of 0.5−0.8.

The final rotation curves of the runs where the disk loses a part of its mass lie, as one would expect, somewhere between the equilibrium (disk + halo) rotation curves and the 'pure halo' rotation curves. However, it is interesting to notice that since in the first case the rotation curves are declining (see Section 4) and in the second case they are rising, one would expect that the 'partial loss' curves should be almost flat! This is indeed the case, as can be seen from the dashed curves in Fig. 6. It is interesting to compare the results of run #4 in Table 3 (upper dashed curve) with those in the top-left panel of Fig. 4. The two rotation curves have exactly the same disk parameters, $(M_d,\ h_d) = (0.03,\ 0.05)$ but the curve resulting from mass loss from an initially heavier disk is flat, while the other is declining. This mechanism offers a solution to the declining rotation curve problem presented by the Hernquist halos.

It remains to be seen, however, whether most luminous spirals have indeed undergone a mass loss comparable to the one needed in this scenario. The star formation rate (SFR) necessary for this can be very roughly estimated by simple arguments. Following the discussion in NEF, the energy required to blow away a fraction f' of the halo mass from a halo with circular velocity V_c is of the order of $f' M_h V_c^2$. Assuming that a fraction ϵ_* of the energy released by supernovae is deposited into the outflow, the star formation (in solar masses) needed to drive the outflow is proportional to $(f'/\epsilon_*)V_c^5$. Assuming a

circular velocity of 150 km/sec, such as the one of the halos of average spirals, this gives a total stellar mass of $7 \times 10^{10}(f'/\epsilon_*)M_\odot$ that has to be formed in a timescale *less* than the dynamical scale of the luminous disk, roughly 10^8 years. Taking a value of 0.05 for f' and an ϵ_* of 0.01 (i.e. that 1% of the energy released by the supernova is deposited to the blowout) this would give an SFR of $4 \times 10^3 M_\odot$/yr. This value is too large for any presently observed galaxy, given for example that the maximum SFR attained by the starburst galaxies observed by Calzetti (1997) is around $400 M_\odot$/yr and that Lehnert & Heckman (1996) have calculated an upper limit in star formation surface density of $20 M_\odot$/yr/kpc^2 for a starburst galaxy. Since we don't really know, however, what physical processes might have occured at the time of the formation of galaxies, this 'partial' baryonic blowout might eventually be a viable explanation of the flat rotation curves.

6 Conclusions

Dark halos with an r^{-1} density peak at the center are by now the standard outcome of high resolution CDM N-body simulations. Very recently, Moore et al. (1997) have produced halos with density singularities as steep as $r^{-1.4}$, in collapse simulations employing $\approx 3 \times 10^6$ particles. It should be noted here that this kind of density peaks, regardless of the fact that they require high resolution in order to be observed, do not really depend on the computational method used. They are due to a fundamental property of cold and collisionless dark matter particles, namely that the phase space density is unconstrained and there is no physically associated scale length; as a result, the dark halos formed will follow power laws in density and will have zero core radii (Moore 1994). If one accepts CDM, which successfully predicts the observed clustering scales for galaxies and clusters (Davis et al. 1985) then the resulting halos have to be made compatible with the properties of the observed HI rotation curves. However, increasingly this compatibility is not supported by the data.

In this paper we simulate baryonic infall inside a dark halo, by adiabatically turning on the potential of an exponential disk inside a spherical system of particles. This halo is represented by spherical and isotropic N-body realizations of two of the γ-models of Dehnen (1993). The γ=1 is the well known Hernquist model that has a central density singularity and the γ=0 model has an (almost) constant density core and resembles an isothermal sphere in the inner parts. The Hernquist profile is a good approximation to the density profiles of CDM halos, especially in the inner parts; we expect that the behaviour of halo models such as the ones of Navarro et al. will be very similar to the Hernquist models in these regions. The values used in our simulations for the visible-to-dark matter ratio and the scalelength ratio span as large a range as possible, within the constraints set by standard CDM cosmogonies. Our conclusions are summarized as follows:

(i) The growth of the disk influences the shape of the halo, causing a non-negligible flattening in the inner parts. The axis ratio reaches a minimum of roughly 0.7 at about 2 disk scalelengths.

(ii) Both halo models acquire larger density gradients at the centre. The new profiles are still well described by the γ-models, but the final value of γ has to be higher than the

initial one. The changes are especially important in the case of the γ_0 model, where the constant density core is destroyed and the initial γ =0 is mapped onto a large range of γ 's, from 0.2 to 1.2 (i.e. even steeper than Hernquist).

(iii) For a galaxy with a Hernquist halo initially, the amount of dark matter inside the Holmberg radius almost doubles due to baryonic infall and the final ratio of luminous to dark matter there is of the order of 0.15 to 0.50; this is true for all plausible scalelength and mass ratios. In other words, the dark matter should already dominate the dynamics at that point. There is a body of evidence which supports the suggestion that the luminous matter dominates in the inner regions of the galaxy, the "maximum disk" hypothesis (van Albada & Sancisi 1986), with the predicted luminous to dark mass ratio at the optical radius having values around 1. This is also supported by Kent's (1987) mass model fits to optical rotation curves, the value found by Kuijken & Gilmore (1989) for the Milky Way and by both maximum disk and best-fit fits to H I rotation curves by Broeils (1992). Hernquist halos give too large a fraction of dark matter inside the optical disk in comparison to these values. This argument, however, has been weakened somewhat since the validity of the maximum disk hypothesis has recently been questioned by Courteau & Rix (1997) on the basis of the Tully-Fisher relation; they argue that the spiral disks are lighter than the maximum allowed mass and that the contribution of the halo is equal to that of the luminous mass already at $2.2h_d$.

(iv) The Hernquist halo, in response to the growth of the disk, gives a total rotation curve that is nowhere flat, for any combination of the parameters; it is always declining beyond a few disk scalelengths, in sharp contrast to the observations of many spiral galaxies. This supports the conclusions of various authors who argued against Hernquist halos, based on their difficulty to explain the kinematics of dwarf spirals. Here we show that this difficulty extends to luminous spirals also. A solution to this problem is rapid mass loss of the protogalaxy through supernova-driven winds (baryonic blowout). Depending on the initial mass, compactness and mass loss percentage of the disk, the rotation curve can become flat or rising, and the halo can even acquire a constant density core which can explain the kinematics of dwarf spirals. For those galaxies, this scenario has been shown to work. However, its plausibility in the case of luminous spirals is questionable because of the fact that the primitive disks must have had either too much mass relative to the halo or a very intense star formation rate to trigger the necessary mass loss.

(v) The γ_0 model, a compromise between the CDM and the isothermal halos, works very well in producing extended flat and featureless rotation curves for a visible to dark matter ratio of 0.03. This happens for a wide range of disk scalelengths, and consequently solves the disk-halo conspiracy problem as far as scalelengths of disk and halo are concerned. It is shown here that the existence of a core in an initial halo model is enough to give a flat rotation curve, without the need for an r^{-2} density profile at large radii and a cutoff radius. Rising rotation curves after baryonic infall, however, such as those observed in dwarf spirals and low surface brightness galaxies cannot be produced by either of the halo models considered in this paper.

These results, especially (iii) and (iv), sharpen the contrast between the way the dark matter is organized in the cosmological CDM simulations and the form that is needed in order to explain the kinematics of spiral galaxies. As a result, one might be prompted to

consider alternative forms of dark matter, or alternative paradigms (Sanders 1990). Hot Dark Matter, for example, does have the necessary phase space constraints to produce the necessary large constant density cores in halos, but has other inherent problems such as difficulty in small-scale structure formation (White et al. 1984). We can conclude by saying that there is not yet an acceptable match between the theoretically predicted halos and the observed rotation curves of spiral galaxies.

References

Antonov V. A., 1962, Vestnik Leningrad Univ., 7, 135
Bahcall J.N., Casertano S., 1985, ApJ, 293, L7
Barnes J., Hut P., 1986, Nature, 324, 446
Barnes J., 1987, in Faber S., ed., 'Nearly Normal Galaxies', Springer-Verlag New York, p. 154
Barnes J., Efstathiou G., 1987, ApJ, 319, 575
Begeman K., 1987, Ph.D. Thesis, Univ. of Groningen
Begeman K.G., Broeils A.H., Sanders R.H., 1991, MNRAS, 249, 523
Becquaert J.-F., Combes F., 1997, A&A, in press
Binney J., Tremaine, S., 1987, *Galactic Dynamics*, Princeton University Press
Blumenthal G.R., Faber, S.M., Flores, R., Primack, J.P., 1986, ApJ, 301, 27
Blumenthal G.R., Faber, S.M., Primack, J.P., Rees, M.J., 1984, Nature, 311, 527
Bosma A., 1978, Ph.D. Thesis, Univ. of Groningen
Broeils A., 1992, Ph.D. Thesis, Univ. of Groningen
Burkert A., 1995, ApJ, 447, L25
Calzetti D., 1997, AJ, 113, 162
Carlberg R.G., Lake G., Norman C.A., 1986, ApJ, 300, L1
Casertano S., van Gorkom J.H., 1991, AJ, 101, 1231
Courteau S., Rix H.-W., 1997, astro-ph/9707290
Davis M., Efstathiou G., Frenk C.S., White S.D.M., 1984, ApJ, 292, 371
Dehnen W., 1993, MNRAS, 265, 250
de Blok W.J.G., McGaugh S.S., van der Hulst J.M., 1996, MNRAS, 283, 18
de Jong R.S., 1995, Ph.D. Thesis, Univ. of Groningen
Dekel A., Silk J., 1986 ApJ, 303, 39
Dubinski J., Carlberg R.G., 1991, ApJ, 378, 496
Fall S.M., Efstathiou G. 1980, MNRAS, 193, 189
Flores R., Primack J.R., 1994, ApJ, 427, L1
Flores R., Primack J.R., Blumenthal G.R., Faber S.M., 1993, ApJ, 412, 443
Hernquist L., 1990, ApJ, 356, 359
Hernquist L., Ostriker J.P., 1992, ApJ, 386, 375
Hjorth J., 1994, ApJ, 424, 106
Jaffe W., 1983, MNRAS, 202, 995
Kalnajs A., 1983, in E. Athanassoula, ed., 'The internal kinematics and dynamics of galaxies', Reidel, Dordrecht, p. 87
Katz N., 1991, ApJ, 368, 325
Kent S.M., 1987, AJ, 93, 816
Kuijken K., Gilmore G., 1989, MNRAS, 239, 571
Lehnert M.D., Heckman T.M., 1996, ApJ, 472, 546
Lynden-Bell D., 1967, MNRAS, 136, 101
Merritt D., 1985, AJ, 90, 1027
Merritt D., Aguilar L.A., 1985, MNRAS, 217, 787

Moore B., 1994, Nature, 370, 629
Moore B., Governato F., Quinn T., Stadel J., Lake G., 1997, astro-ph/9709051, ApJ, in press
Navarro J.F., Frenk C., White S.D.M., 1995, MNRAS, 275, 720
Navarro J.F., Frenk C.S., White S.D.M., 1996, ApJ, 462, 563
Navarro J.F., Eke V.R., Frenk C.S., 1996, MNRAS, 283, L72
Ossipkov L.P., 1979, Soviet Astron. Lett., 5, 42
Ryden B., Gunn J.E., 1987, ApJ, 318, 15
Sackett P.D., Sparke L., 1990, ApJ, 361, 408
Sanders R.H., 1990, A&AR, 2, 1
Sanders R.H., Begeman K.G., 1994, MNRAS, 266, 360
Shu F.H., 1978, ApJ, 225, 83
Tremaine S. et al., 1993, AJ, 107, 634
Trimble V., 1987, ARA&A, 25, 425
van Albada T.S., Bahcall J.N., Begeman K., Sancisi R., 1985, ApJ, 295, 305
van Albada T.S., Sancisi R., 1986, Phil. Trans. R. Soc. London, A2330, 447
van Albada T.S., van Gorkom J., 1977, A&A, 54, 121
van Albada T.S., 1982, MNRAS, 201, 939
Walker T.P., Steigman G., Schramm D.N., Olive K.A., Kang H.S., 1991, ApJ, 376, 51
White S.D.M., Rees M.J., 1978, MNRAS, 183, 341
White S.D.M., Davis M., Frenk C., 1984, MNRAS, 209, 27

A Stability of anisotropic models

In this Appendix we investigate the stability of anisotropic Hernquist halos, and briefly discuss disk growth inside these halos. We deal with Ossipkov-Merritt type anisotropy (Ossipkov 1979, Merritt 1985) where the distribution function depends on the energy and the angular momentum in a certain way: $f = f(Q)$ where $Q = E - L^2/2r_a^2$. In this expression E is the energy, L is the angular momentum and r_a is the so-called anisotropy radius that determines the degree of velocity anisotropy through the relation

$$\frac{\sigma_r^2}{\sigma_t^2} = 1 + \frac{r^2}{r_a^2}, \tag{9}$$

where σ_r and σ_t are the radial and tangential velocity dispersions respectively. As $r_a -> \infty$ the system becomes isotropic, while $r_a = 0$ gives purely radial orbits. The orbits are in general isotropic in the center and become progressively radial outward for $r > r_a$. For sufficiently small r_a this gives rise to the well known radial orbit instability that results in the formation of a bar. The onset of instability has been extensively studied by Merritt & Aguilar (1985) for Jaffe (1983) systems ($\gamma = 2$). An analogous study of Hernquist models, however, that have a much wider range of applications–bulges of spirals, elliptical galaxies and dark halos–is still lacking. Apart from this, there are a few more reasons to study the anisotropy in these systems. First, a radial anisotropy has indeed been found in the systems that result from collapse and violent relaxation simulations (van Albada 1982, Carlberg, Lake & Norman 1986). Second, the radial orbit instability and the subsequent bar formation might be related to the very flat halos found in some studies (Sackett & Sparke 1990, Becquaert & Combes 1997). Finally, it would be of interest to consider the effect of disk formation inside marginally stable dark halos.

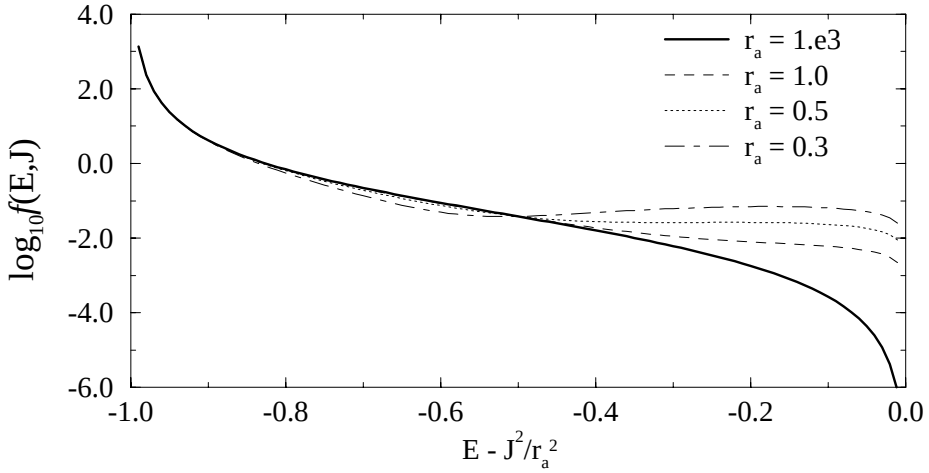

Figure 1: The phase space distribution function $f(Q)$ as function of $Q = E - L^2/(2r_a^2)$ for various values of the anisotropy radius r_a. The thick solid line corresponding to r_a=1000, is the isotropic DF.

Our main objective here is to establish the minimum anisotropy radius r_a or, alternatively, the maximum ratio of radial to tangential kinetic energies, $2T_r/T_t$ for which the system is stable. A first estimate for the critical r_a is given by Hjorth's (1994) extension to Antonov's (1962) first law for the stability of isotropic systems, $df/dE < 0$. Hjorth's criterion reads $df/dQ \leq 0$, where Q is defined as in the previous paragraph. In Fig. A2.1 we plot the distribution function of the Hernquist model as a function of Q for anisotropic radii of 1000, 1.0, 0.5 and 0.3. The model with $r_a = 1000$ is essentially isotropic. It is easy to see that the DF for $r_a = 0.5$ is marginally monotonic, while the DF for $r_a = 0.3$ is not; its derivative changes sign at around $Q = -0.55$. The instability, therefore, should begin somewhere near $r_a = 0.5$. We subsequently create models with $r_a = 0.5$, 0.4, 0.3 and 0.25 and let them evolve (0.25 is the smallest possible anisotropy radius; beyond this the DF is not everywhere positive). The total mass and Hernquist radius are, as before, equal to 1 and the number of particles is 32,000. The final state of these models, at t=30, is shown in Fig. A2.2. The $r_a = 0.5$ and $r_a = 0.4$ models seem to be stable to eye inspection. The bar instability is very clear, however, for $r_a < 0.4$; as noticed also by Merritt & Aguilar (1985) its onset is quite abrupt. For $r_a = 0.25$ a conspicuous prolate bar is formed already by t=15 and remains roughly unchanged from there on. We should notice here that the SCF code is not very well suited to handle systems that are far from spherical symmetry, such as this one. For this reason we repeat the $r_a = 0.25$ run using a standard TREECODE (Barnes & Hut 1986) and the results appear to be qualitatively the same. In Fig. A2.3 we show the run of axis ratio (c/a) as a function of time, measured at the radius that includes half of the total number of particles. Here it can be seen that the $r_a = 0.4$ model is as a matter of fact also unstable, thus setting the stability limit to $r_a = 0.5$, in good agreement with the prediction of Hjorth (1994). The strength of the bar depends on the anisotropy radius; it is in general prolate or slightly triaxial, with axis ratios 1:0.85:0.80 for $r_a = 0.4$ to 1:0.60:0.52 for $r_a = 0.25$. Finally, a few words about disk growth in anisotropic halos. A

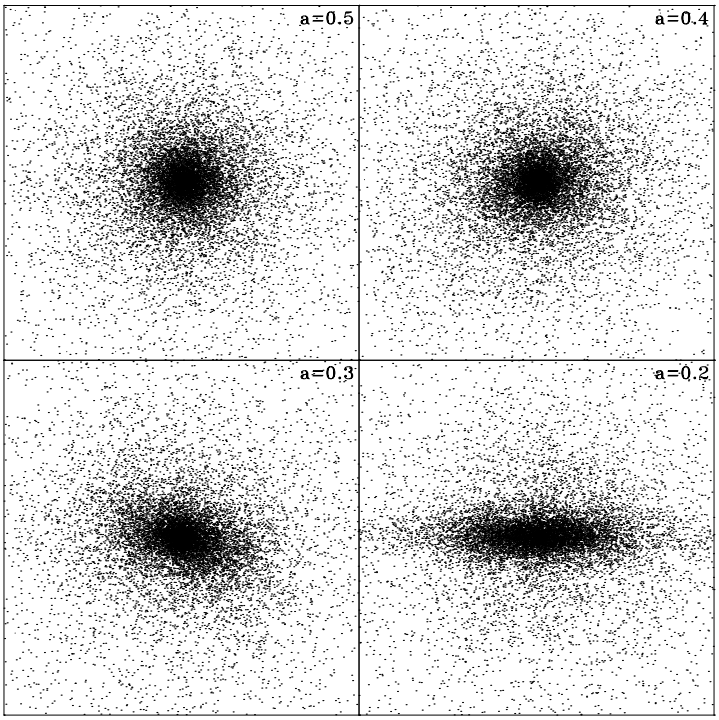

Figure 2: Face-on views of the *final* state of 4 models with various degrees of anisotropy. The models have been undersampled by a factor of 4 for clarity, so only 25% of the real number of particles are shown here.

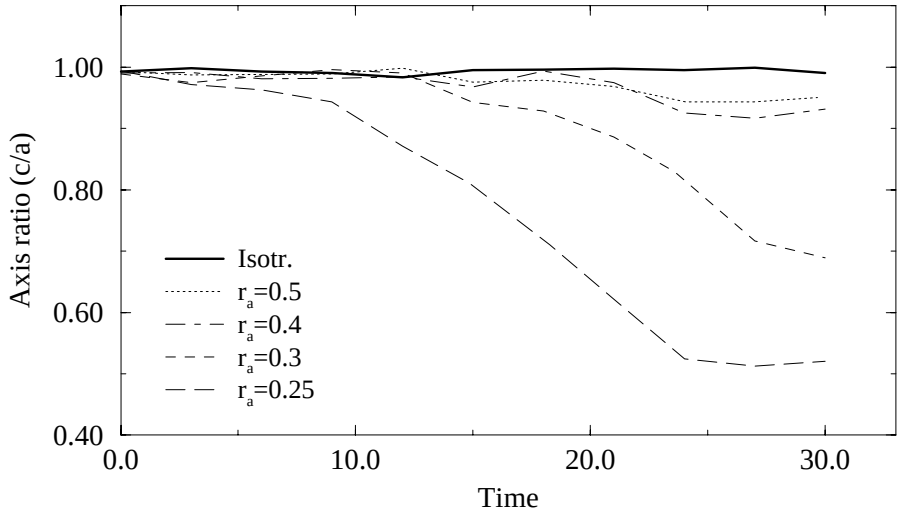

Figure 3: Time evolution of the axis ratio c/a for the anisotropic models.

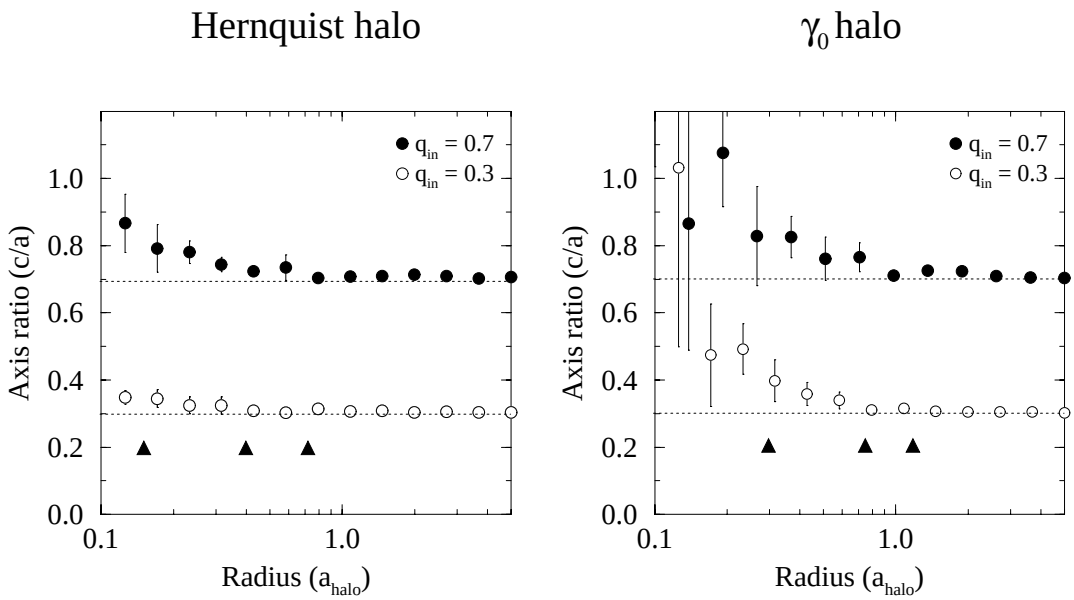

Figure 4: Axis ratio as a function of radius for two data sets with pre-defined ellipticities. The input axis ratios are shown by the dotted lines. The error bars are the standard deviations from measuring the axis ratio at that particular radius on 5 different realizations of the same model. The black arrows indicate the radii that include 1000, 5,000 and 10,000 particles.

disk of mass $0.03M_h$and scalelength $0.05a_h$is grown inside the two marginally stable halo models, with r_a of 0.5 and 0.4. The stability and shape of the halo do not appear to be significantly affected. The flattening of the inner parts is the same as in the isotropic cases of §3.1, but further than that no other remarkable effects are observed, in the sense that the bar instability of the halo proceeds in the same way as if there were no disk at all.

B The accuracy of the axis ratio determination

In order to assess the reliability of the method for the determination of the axis ratio, we do some tests using models with a certain fixed ellipticity. We create oblate Hernquist and γ_0 halos consisting of 66,000 particles, with two different axis ratios (c/a), 0.7 and 0.3. This is done by simply mapping the *particle positions* of the respective spherical models to an ellipsoidal configuration. These are not self-consistent models; the construction of such models is not possible at this moment.

For each model 5 N-body realizations are made, each with a different random number seed. The axis ratio is then measured as a function of radius using the iterative diagonalization of the inertia tensor, and the results for each realization are averaged to give a final c/a profile. The results are shown in Fig. B1, where the error bars indicate the standard deviation of c/a at each radius. As we can see, the reliability of the method depends heavily on the number of particles involved. The ellipticity is always underestimated near the center, but the axis ratio then converges rather quickly to the input value. For the Hernquist model, with a steep density gradient, the errors at radii including 1000, 5,000

and 10,000 particles are of the order of 10%, 1% and less than 1% respectively. The results for the γ_0 are the same, except for the 1000 particles radius; the error there is around 15%. The errors at small radii for the γ_0 model are as a rule much larger, owing to the small number of particles that "live" in the constant density core. In general, however, the results are satisfactory. It should also be born in mind that the halos with a disk described in the text will have smaller errors at small radii, as the presence of the disk increases the number of particles there.